Research Article | Vol. 10, No. 9 / 1 September 2019 / Biomedical Optics Express 4896
Biomedical Optics EXPRESS

Visualization of skin capillaries with moving red blood cells in arbitrary area of the body

NIKITA B. MARGARYANTS,[1] IGOR S. SIDOROV,[1] MIKHAIL V. VOLKOV,[1] IGOR P. GUROV,[1] OLEG V. MAMONTOV,[1,2] AND ALEXEI A. KAMSHILIN[1,*]

[1] *Faculty of Applied Optics, ITMO University, 49 Kronverksky pr., 197101, St. Petersburg, Russia*
[2] *Department of Circulation Physiology, Almazov National Medical Research Center, 2 Akkuratova st., 197341, St. Petersburg, Russia*
[*] *alexei.kamshilin@yandex.ru*

Abstract: Evaluation of skin microcirculation allows for the assessment of functional states for neuroendocrine and endothelial regulation. We present a novel method to visualize skin microvessels in any area of the body, which is in contrast to classical capillaroscopy, in which the application areas are limited to the nailfold and retina capillaries. The technique is based on microscopic video-image analysis. It exploits a specific feature of irregularity of red-blood-cells motion. Feasibility of the method is demonstrated by mapping the skin capillaries in the forearm and face of 11 healthy volunteers. The proposed method is promising for the quantitative assessment of cutaneous microcirculation in a wide range of diseases and functional states.

1. Introduction

Study of local microcirculation disorders is of high importance for development of early diagnosis methods of different diseases such as scleroderma and other rheumatologic and dermatologic diseases. The timely diagnosis of neoplastic skin processes is also important. The earlier microcirculation disorders are detected, the greater the chances of preventing possible complications of a disease and to start in time an effective treatment. At present most microvascular studies are made combining the microscope with a video camera thus providing evaluation of static and dynamic conditions of microvessels [1–3]. The technique is referred to as capillaroscopy allowing excellent images of the red blood cells (RBCs) in the capillaries to be obtained [4–7]. Notably that the most of experiments dealing with RBCs visualization have been performed with the nailfold capillaries [6–9]. However, from the point of view of medical diagnostics, it would be much more informative to measure and analyze the state and morphology of capillaries in proximal locations, i.e. closer to the heart [10] or at the site of skin lesions. Unfortunately, no successful visualization of skin capillaries situated in sites other than fingernails has been reported. Observations of the capillary bed in proximal locations is significantly challenging task because of thick epidermis, hairs, wrinkles, nevi, and problems in focusing of microscopic images.

In this paper, we report on novel approach in visualization of skin capillaries with moving RBCs, which can be used in arbitrary area of the body. Analysis of dynamic parameters of green-light interaction with tissue allowed us to distinguish capillaries particularly from the skin irregularities.

2. Visualization method

2.1. Recording of microscopic images of subject's skin

Microscopic images of the skin were recorded by using a custom-made microscope schematically shown in Fig. 1. It consisted of two reverse connected lenses: zoom lens Canon EF with the

#372115 https://doi.org/10.1364/BOE.10.004896
Journal © 2019 Received 8 Jul 2019; revised 18 Aug 2019; accepted 22 Aug 2019; published 30 Aug 2019

Biomedical Optics EXPRESS

focal length of 70–300 mm and short-focus lens MIR (JSC VOMZ, Russia) of high F-number, numerical aperture of 0.17 and the focal length of 37 mm. The optical scheme of the microscope made it possible to record video frames of the subject's skin area sizing from 1.3×0.8 to 5.6×3.5 mm^2. The area under study was illuminated at four projection angles (about 45 from the normal to the skin) by the green light of light-emitted diodes (LEDs) operating at the wavelength of 525 ± 30 nm (power of 3 W). Such multiangle arrangement of LEDs provided uniform illumination of the skin area avoiding shadows from individual hairs, folds or irregularities. A polarization film covered each LED so that the linearly polarized light illuminated the skin area under study. Another polarization film with transmission axes orthogonal to the illuminating polarization was attached to the zoom lens. Such a polarization arrangement reduces the skin specular reflections and motion artefact influence on the detected signals [11]. A digital monochrome CMOS camera (10-bit model USB3.0 uEye 3060CP of the Imaging Development System GmbH) was used to record all the videos in presented experiments at the frame rate of 50 fps and frame size of 1200×1200 pixels.

Fig. 1. Layout of the custom-made video-capillaroscopy setup providing visualization of capillaries in the forearm as an example.

An area of the body to be studied usually differs from the plain shape. Due to small focal depth of our microscope, it is sensitive to focusing plane position over the observation area of 2.5×2.5 mm^2. Moreover, involuntary skin displacements (including these in the vertical direction)

Biomedical Optics EXPRESS

are inherent in every living object. They can lead to time-varying image defocus, and thus to motion-related modulation of the pixels value. To diminish the influence of skin displacement, the microscopic images were recorded through a glass plate gently contacted subject's skin (Fig. 1). The glass allowed us to increase skin planeness, reduce the likelihood of image defocusing, and decrease local displacements in the horizontal plane during the measurements. In addition, the skin transparency was augmented by an application of immersion oil between skin and glass [4,6]. Specular reflections from the glass and oil were suppressed by polarization filtration [12].

2.2. Participants and experimental procedure

We recruited 11 volunteers (8 males, 3 females) between 21 and 49 years (27 ± 9 years). Each subject was informed about the experimental procedure and gave written consent on participation in the experiment. The study was conducted in accordance with ethical standards presented in the 2013 Declaration of Helsinki. The study plan was approved by the ethical research committee of the Almazov National Medical Research Centre prior the experiments. The most of the experiments were performed aiming to visualize capillaries in the forearm area. In addition, capillaries were visualized in the forehead and cheek areas of five subjects.

It should be noted that some of subjects experienced serious problems in keeping their body motionless. To achieve successful capillaries visualization even in these cases, we adopted the protocol in which the microscopic video was recorded during three minutes, and then a 10-s interval less affected by body's motion was selected for data processing. In the case of study capillaries in the forearm area, subject was sitting in a comfortable position with the hand at the heart level laid on a rigidly fixed support. Alternatively, a subject was in supine position when visualizing capillaries on both cheek and forehead. All measurements were carried out in a laboratory maintained at a temperature of 22–24 °C.

2.3. Image and data processing

Evaluation of conventional nailfold microscopic images includes three main steps [8,13]: (i) compensation of involuntary subject's motion, (ii) selection of the frames range, the least distorted by motion artefacts, and (iii) estimation of a parameter characteristic of capillaries. In contrast to images of nailfold capillaries [5–9], skin capillaries in other parts of the body are difficult to distinguish against the background of other skin features. An example of the microscopic image of the forearm skin is shown in Fig. 2(a). Our technique of the data evaluation involves the same aforementioned steps but the image parameter used to distinguish capillaries from other tissue differs from that adopted in other works. The order and detailed description of the algorithm steps are given in the following subsections of the paper.

Colored squares show position of regions of interest (ROI) in which particular realizations of photoplethysmographic (PPG) waveforms will be demonstrated as examples. Dynamics of the pixel value averaged over the whole frame and corresponding PPG waveform are presented in Fig. 2(b).

The set of PPG waveforms calculated in every pixel can be considered as an ensemble of realizations of a random process. To assess such random realizations numerically, it is possible to calculate a mean value over the ensemble as well as a variance (dispersion) by processing the PPG waveform in the time domain. However, periodical variations are inherent in the PPG waveforms. That is why evaluation of their spectral properties in frequency domain is of high importance. From the viewpoint of reemitted light intensity consideration, the most informative is the PPG waveforms power spectrum. Following to well-known theory of random processes, the PPG waveforms dispersion can be calculated via integration of the power spectrum over the frequency range. Below we will follow to this spectral approach.

Biomedical Optics EXPRESS

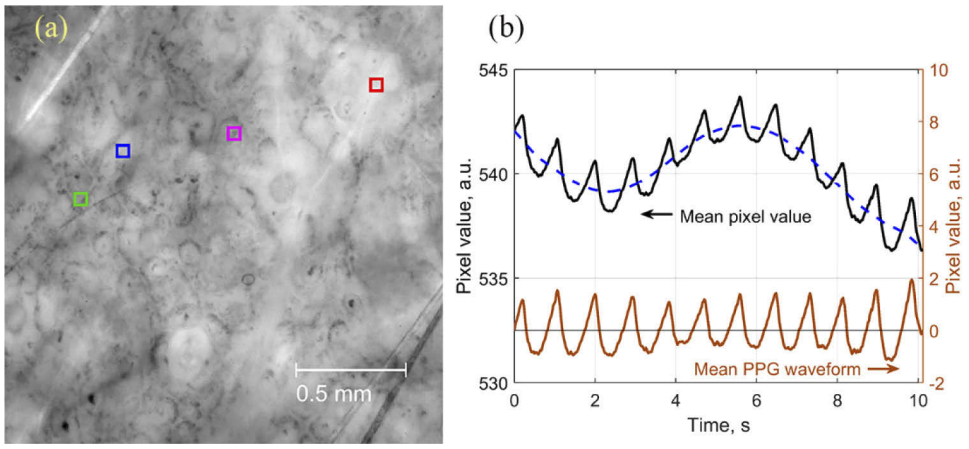

Fig. 2. An exemplary frame of recorded microscopic image (a) and evolution of the pixel value averaged over the whole frame (b). The arrows in the panel (b) indicate the respective axes of the presented graphs.

2.3.1. Selecting an interval with the least motion

To select the 10-s interval with the least motion artefacts, we estimated variability of images under the criterion of frame-by-frame evolution of the pixel mean value calculated over the whole frame. The frame range within which variations of the mean pixel value are minimal is supposed to be an interval with smaller relative motion between subject's skin and microscope. Typical graph of raw, non-filtered mean pixel dynamics is shown in Fig. 2(b) by black line. After subtracting the slowly varying trend (dashed blue line), the dynamics of the mean pixel value is expressed by the brown line in Fig. 2(b), which is referred to as PPG waveform [14,15]. It is clearly seen that the mean pixel value, which is proportional to the light intensity reemitted from the skin, is modulated at the heartbeat frequency. Peaks in this waveform take place at the end of the diastole phase of the pulse wave [15]. This waveform will be used in the next steps for suppression of the heart-related oscillations. These oscillations inherent in the PPG waveforms everywhere over the skin and they have to be suppressed to recognize a capillary via other attributes of the reemitted light as it is considered below.

2.3.2. Skin motion compensation

Our approach of capillaries visualization is based on the analysis of time-varying characteristics of the light reemitted from the skin. However, this is a challenging task because the dynamic parameters related to moving RBC in capillaries are to be identified against the background of interference created by various micro-movements of the epidermis and dermis. This requires careful compensation of any image displacement during the chosen interval for the analysis. In the proposed algorithm, this was achieved by selecting a rectangular mask and its subsequent displacement to compensate for the skin motion. Rectangular mask smaller than the frame size was located in the center of the first recorded frame. Once per cardiac cycle we evaluated image displacement by using the method of phase correlation (the ***imregcorr*** function in Matlab). It was done when the mean PPG waveform [brown line in Fig. 2(b)] reached its next peak. Then the mask was translated to compensate the estimated displacement. The size of the mask was set so that it is remaining within a frame even for the maximal image displacement during the selected interval.

The mask was divided into small ROIs with the size of 2×2 pixels each corresponding to an area of 4.1×4.1 μm^2. Every ROI was chosen to have a common border with adjacent ROIs

Biomedical Optics EXPRESS

without overlapping. Position of each small ROI was shifted in respect to the skin microscopic image following the mask displacement so that the ROIs were linked with local skin features. Frame-by-frame evolution of the mean pixel value was calculated in every small ROI within the time interval of 10 s. Examples of the mean pixel value evolution calculated in ROI marked by colored squares [see Fig. 2(a)] are shown in Fig. 3(a). Localization of these ROIs was chosen after visual inspection of a video presented in the Visualization 1. Note that the video was made up involving the frames in which translational displacement is compensated. One can clearly see several areas in the video in which moving dark spots are observed. We identify these spots as moving RBCs and their aggregates. Two ROIs [red and pink in Fig. 2(a)] were located in areas with moving RBCs, whereas other two [blue and green in Fig. 2(a)] were in the areas free of moving RBC. As seen, the light is modulated at the heartbeat frequency (about 1 Hz) in the both kinds of the selected ROIs. While the modulation looks like regular in areas without moving RBC [blue and green curves in Fig. 3(a)], it is far rather randomly modulated in the areas with RBCs [red and pink curves in Fig. 3(a)].

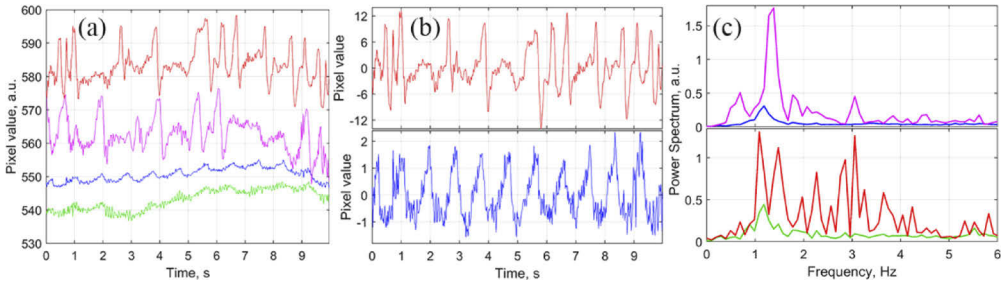

Fig. 3. Particular realizations of PPG waveforms and their spectra. (a) Evolution of the mean pixel value estimated in four selected ROIs: red and pink are in the areas with moving RBCs, whereas blue and green – without. (b) PPG waveforms in the red and blue ROIs. (c) Power spectra of PPG waveforms in all four selected ROIs. Color of the graphs corresponds to the color of the squares marking ROI position in Fig. 2(a).

After removal of slow varying changes (by the operations similarly with the ones applied to the mean pixel value of the whole frame, Sect. 2.3.1), PPG waveform at every small ROI was calculated. For clarity of presentation, only two representative PPG waveforms (one from the area with moving RBCs, another – without) from respective ROIs (red and blue) are shown in Fig. 3(b). Power spectra of four PPG waveforms corresponding to the selected ROIs are shown in Fig. 3(c) by curves of the same color as squares in Fig. 2(a). Notably that while the spectra of PPG signals estimated in areas without RBC (blue and green) are similar, the other two (red and pink) differ from each other. We suggest that this difference might arise from speed variations of RBCs and their aggregates in different capillaries. Particularly in the red and pink ROIs, the modulation maxima are observed at 1.0 and 1.3 Hz, respectively; both are different from the heart rate (1.1 Hz).

Despite the differences in light modulation estimated in different ROIs with moving RBCs, the spectra of PPG waveforms in them are significantly different ($p < 0.0001$) from those in ROIs without RBC. This difference becomes evident in Fig. 4(a) where we plotted the brown curve as averaged over 50 particular power spectra estimated in randomly chosen ROIs with moving RBCs against the dark blue curve representing the mean spectrum over 50 other ROIs without RBC. One can see in Fig. 4(a) that the power spectrum of reemitted light from moving RBCs covers much wider spectral band with respect to other tissue areas. The mechanism initiating the difference between the spectra is considered below.

Biomedical Optics EXPRESS

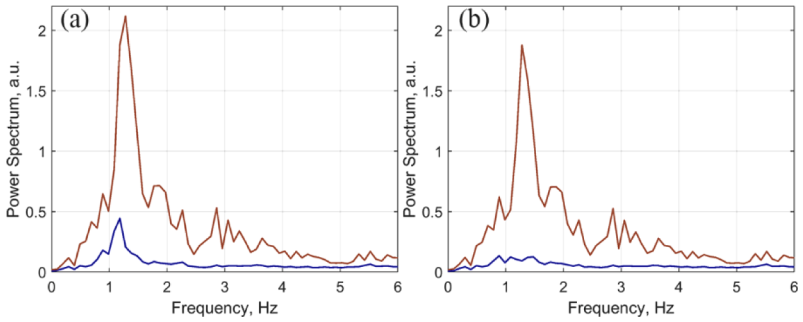

Fig. 4. Mean power spectra of PPG waveforms. (a) Averaging over 50 randomly chosen ROIs localized in the areas with moving RBCs (brown curve) and over other 50 ROIs localized in the areas without moving RBC (dark blue curve). (b) Similar graphs as in the panel (a) but the spectra from the same ROIs were averaged after suppression of the heart-related modulation.

2.3.3. Capillary visualization using difference in PPG waveform spectra

As seen in Fig. 4(a), the maximum of the light modulation is achieved at the heart rate (1.1 Hz) in majority of arbitrarily selected ROIs situated in the both areas with running RBCs and without. It is worth noting that the relative amplitude of the PPG-waveform modulation at the heart rate in the ROI localized at the capillary is just slightly higher than in other places. Therefore, it is hard to be used as a specific parameter capable for distinguishing a capillary from the rest of the tissue. We hypothesize that such amplitude similarity could be explained in the frames of the recently proposed model of PPG signal formation [12]. According to this model, the light is modulated mainly due to compression/decompression of the capillary bed occurring synchronously with changes of blood pressure in vessels located nearby the place of the measurement. Blood pressure pulsations in deeply located arteries and arterioles result in displacement of epidermis. Even though such a displacement is rather small, it might lead to variations of pixel value because of defocusing due to inevitably short focal length of the microscope with high F-number and the accompanying contrast degradation when imaging skin features. In the alternative model [16], the light modulation is explained by ballisto-cardiographic effect in which the light modulation arises from variations of the reflection angle from the epidermis surface. Both models predict occurrence of light modulation in the areas situated out of skin capillaries.

Nevertheless, particular power spectrum of PPG waveform in the ROI at the capillary area differs from that at other area as shown in Fig. 3(c). Whereas the PPG waveform in any area without moving RBC has a sharp peak at the heart rate, the power spectrum of the waveform from the capillary is significantly broadened. We suggest that the spectrum broadening arises from inhomogeneity of RBCs density in capillaries and their movement. Some of RBCs are joint together forming aggregates of different length [17]. When these aggregates separated by plasma (which absorb green light less than RBC) are moving in capillaries, they produce light flickering, as it is demonstrated in the Visualization 1. Since the speed of RBC in capillaries is modulated at the heart rate [5,18], the main spectral peak is observed at the heartbeat frequency. Varying lengths of the RBC aggregates results in broadening of this peak due to high-frequency random intensity modulation caused by the moving RBC aggregates. It should be underlined that the PPG waveforms spectra evaluated in areas without moving RBC are similar each other as well as with the spectrum of mean waveform over the whole frame.

To enhance the properties of the PPG-waveform spectra in capillaries marked out above, we propose to calculate the difference between the normalized PPG waveform of a ROI [such as shown in Fig. 3(b)] and the waveform averaged over the whole frame [brown curve in Fig. 2(b)].

Biomedical Optics EXPRESS

We will assign below this difference as the PPG differential waveform (PPG-DW). Two power spectra averaged over the spectra of particular PPG-DW estimated at the same ROIs as for spectra evaluation before compensating the heart-related modulation are shown in Fig. 4(b). Significant difference between the PPG-DW mean spectrum in capillaries and that in other tissue is clearly seen at the range between 0.6 and 6 Hz.

By calculating the standard deviation (STD) of the PPG-DW in a ROI within the low-frequency range after removal of the heart-related modulation, we obtain a parameter called as flickering index (FI) that has allowed us to visualize the skin capillaries with moving RBCs in arbitrary area of the body.

3. Results

3.1. Visualization of skin capillaries in the forearm

The light flickering in capillaries (which is estimated by FI) depends on the RBC speed, which varies among capillaries [5]. Moreover, it is varying from one subject to another. To estimate quantitatively how the capillaries are distinguished from the tissue, we calculated the dispersion of the PPG-DW over 50 small ROIs situated at capillaries [representative mean spectrum is shown in Fig. 4(b) by brown curve] and compared it to the dispersion of PPG-DW over 50 small ROIs at the tissue. PPG-DW dispersions were estimated for each subject in 10 arbitrary chosen big ROIs. While choosing these areas, we manually identified the areas in microscopic images spoiled by highly contrast hairline artefacts that were distinguished from the capillaries by their morphology. These artefacts were not included in the big ROIs. The affiliation of a small ROI to either a capillary or a tissue without moving RBC was determined by viewing every respective video, such as presented in the Visualization 1. The mean PPG-DW dispersion ± STD is summarized in Table 1 for every subject. Demography of subjects is also listed in Table 1.

Table 1. Power spectrum dispersion measured in the forearm

Subject	Gender	Age, years	Area	PPG-DW dispersion (capillaries)	PPG-DW dispersion (tissue)	Figure
AAB	female	22	forearm	82 ± 4	2.36 ± 0.06	-
AOL	male	22	forearm	112 ± 26	2.84 ± 0.05	Fig. 5(a)
AVE	female	27	forearm	55 ± 16	2.30 ± 0.04	Fig. 5(b)
DES	female	22	forearm	305 ± 156	2.46 ± 0.03	Fig. 5(c)
DGO	male	21	forearm	46 ± 16	2.39 ± 0.10	Fig. 5(d)
MAK	male	22	forearm	200 ± 37	2.32 ± 0.03	Fig. 5(e)
MDH	male	22	forearm	24.2 ± 4.2	2.09 ± 0.07	Fig. 5(f)
NBM	male	49	forearm	39 ± 14	2.91 ± 0.16	Fig. 5(g)
PSS	male	35	forearm	55 ± 10	2.84 ± 0.09	Fig. 5(h)
VEB	male	23	forearm	144 ± 21	2.91 ± 0.12	-

As seen in Table 1, the mean PPG-DW dispersion in the tissue without moving RBC is about the same for all subjects under study (between 2.1 and 2.9), whereas the mean dispersion in the capillaries varies for more than order of value (from 24 to 305). Anyway, the PPG-DW dispersion in areas with moving RBCs is at least ten times greater than this parameter in other areas. The ratio of the PPG-DW dispersions in capillaries to that in other tissue points can be interpreted as a signal-to-noise ratio in the capillary recognition problem. We assume that in subjects with higher PPG-DW dispersion, a greater number of RBCs move near the epidermis at a higher speed. In other words, this parameter characterizes the perfusion of blood in the skin capillaries. Nevertheless, no correlation of the mean PPG-DW dispersion in the areas of capillaries with either gender or age of subjects has been observed.

Biomedical Optics EXPRESS

Figure 5 shows examples of visualized capillaries for eight subjects evaluated in the forearm areas. Each panel in Fig. 5 consist of initial microscopic image of the skin and corresponding distribution of capillaries. Capillaries are visualized by using FI, which is coded in pseudo colors with the scale shown on the right of each map. One can see that the morphology of capillaries differs from one subject to another. Since skin capillaries are oriented typically orthogonal to the skin surface, their loops are observed more frequently. However, several capillaries partly oriented in the plane of view have been observed in two subjects as seen in Fig. 5(d, g).

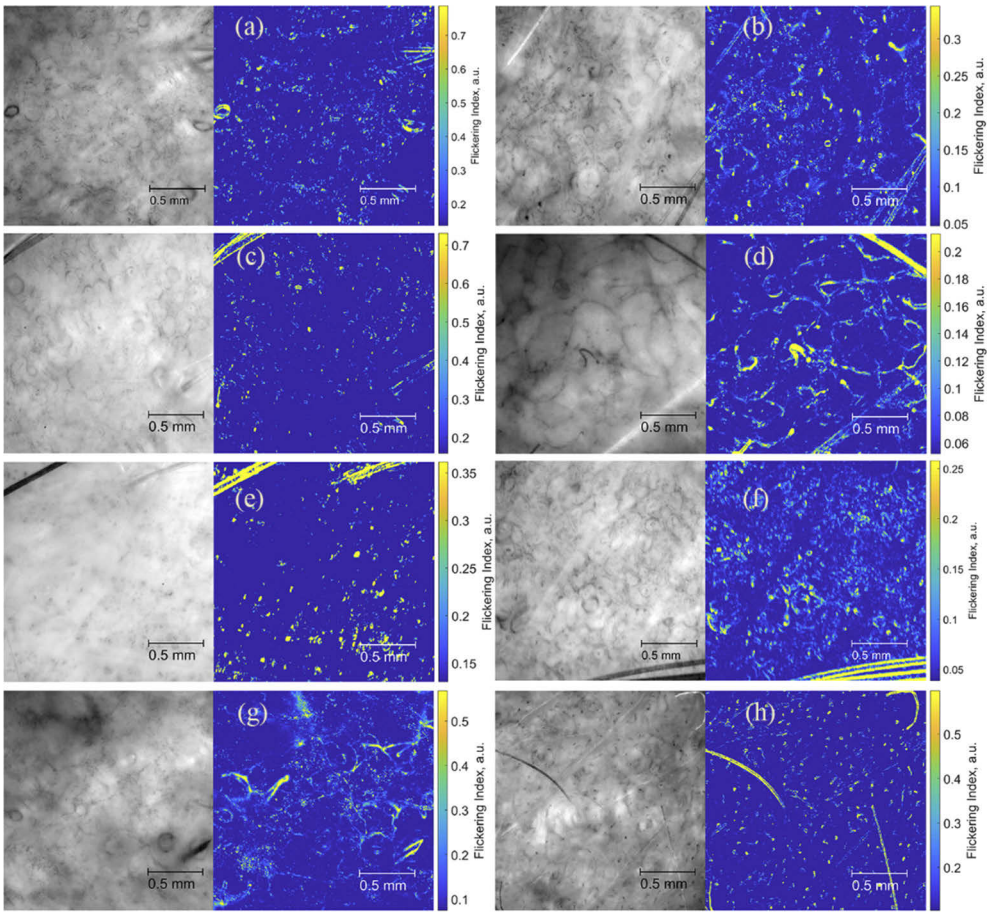

Fig. 5. Microscopic images of the skin in the forearm and corresponding distribution of capillaries with moving RBCs. Demographic data of the subjects are listed in Table 1. Color scales on the right of each panel show the parameter FI.

3.2. *Visualization of capillaries in the cheek and forehead*

The proposed method allows visualization of the skin capillaries not only in the forearm area, but also in other parts of the body, for example, on the forehead and cheek, as shown in Fig. 6 with the obtained data summarized in Table 2. Interestingly, the average PPG-DW dispersion outside the capillaries remained at about the same level as in the measurements on the forearm. However, this indicator in the areas with moving RBC is significantly larger in the facial area than in the forearm (cf. Table 1 with Table 2). A higher density of capillaries in the facial area than on the hands [14] may be particularly the cause of this difference. It is worth noting that

Biomedical Optics EXPRESS

microscopic images of the skin of the face are much more difficult to keep still during the video recording. This increases the requirements for image stabilization accuracy, thus extending the data processing time.

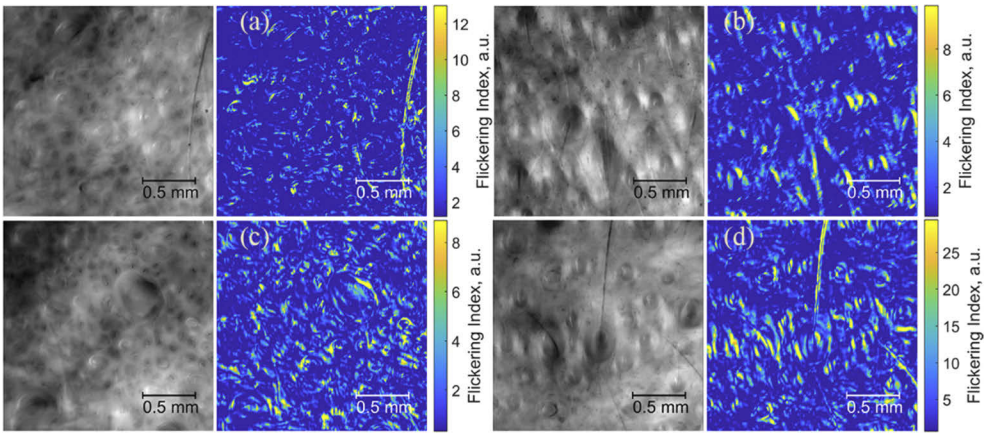

Fig. 6. Microscopic images of the skin in the facial area (upper row – areas in cheeks, lower row – areas in the forehead) and corresponding distribution of capillaries with moving RBCs evaluated for two subjects: left column – subject MAK; right column – subject ZAA (see Table 2 for details). Color scales on the right of each panel show the parameter FI.

Table 2. Power spectrum dispersion measured in the facial area (cheek and forehead)

Subject	Gender	Age, years	Area	PPG-DW dispersion (capillaries)	PPG-DW dispersion (tissue)	Figure
MAK	male	22	cheek	880 ± 170	2.44 ± 0.13	Fig. 6(a)
ZAA	male	22	cheek	1100 ± 450	3.36 ± 0.25	Fig. 6(b)
MAK	male	22	forehead	480 ± 180	2.13 ± 0.14	Fig. 6(c)
ZAA	male	22	forehead	730 ± 130	3.71 ± 0.56	Fig. 6(d)

Spatial distributions of the flickering index representing position of moving RBCs were obtained in areas of forearm, cheek, and forehead for different subjects. These maps presented in Figs. 5, 6 side-by-side with initial microscopic images confirm feasibility of the proposed technique to visualize capillaries in any area of the body.

4. Discussion

In this work, we demonstrate the first attempt of mapping the capillaries with moving RBCs beyond the traditional areas suitable for conventional capillaroscopy. There are no restrictions on the skin areas in which this method can be applied. Capillaries are visualized due to difference in spectral parameters of the green light after its interaction with irregular moving RBCs in respect to those parameters of other tissues. Microvasculature visualization in vivo has practical and theoretical importance for both diseases diagnosing and studying their pathogenesis [19]. Quantitative estimation of microcirculation changes occurred during the disease treatment is also of high importance. The proposed method allows solution of these problems, thus having prospects for more accurate diagnosing of such diseases as scleroderma, which relates to small vessels sclerosis, and possibly Raynaud's syndrome of another etiology characterized by reduction of the vascular blood flow. Moreover, it can be useful for diagnosing and monitoring the treatment of the diabetes mellitus because this disease in the stage of decompensation also leads to the

Biomedical Optics EXPRESS

microvasculature destruction [20]. We also assume that the method can be useful for identifying skin neoplasms.

It should be emphasized that our algorithm visualizes exclusively capillaries with moving RBC. If during the selected observation interval (10 s in our experiments) RBCs are not moving in a capillary, it could not be distinguished from other tissue. Similarly, when the RBC speed in a capillary is so fast that it is displayed for a distance exceeding its size within the frame accumulation time, light flickering is diminished, and the capillary is not visualized, as well. Light flickering also depends on the focusing on the microscopic image. The depth of focusing of our microscope is 36 μm. Microvessels situated deeper in the dermis than the focal depth are not visualized by our technique because defocused RBCs do not contribute to light flickering. Therefore, only parts of the capillaries close to the epidermis can be visualized by the proposed method.

Note that the observed flickering rate depends on both the RBC speed and frame rate of the video recording. The frame rate should be set so that the displacement of RBC moving in capillaries with the mean speed is to be resolved in neighboring frames. In our experiments, the frame rate of 50 fps satisfied this condition when measuring forearm in all subjects but it was increased to 100 fps for measuring at the facial area.

At the present stage, it is difficult to differentiate a number of details of the skin pattern from microvessels, based only on the proposed FI parameter, and it is likely that identification supplemented by morphological criteria is required. This is the task for the near future research. At the same time, the principle of differentiation capillary with moving RBCs from the other tissue on the basis of this important criterion gives significant results, allowing us to significantly simplify the visual assessment of the functional state of the skin.

Currently no quantitative criteria have been developed to identify the norm and pathology in microcirculation. Nevertheless, by applying basic tests for enhance / reducing blood flow and measuring the response of skin capillaries by the proposed method, it is possible not only to assess the state of microcirculation of the skin at rest, but also under physiological stress. This allows determination of the reserve potential of the blood vessels, as well as the state of the neurogenic and endothelial regulation [21]. Consequently, the technique could be applied to study reaction of microcirculation to various functional tests, which change the blood perfusion in skin.

Funding

Russian Science Foundation (15-15-20012); Ministry of Education and Science of the Russian Federation (8.2501.2017/4.6).

Acknowledgments

The research was supported by the Russian Science Foundation (RSF) (grant 15-15-20012) in terms of theoretical formulation of the approach including developments of the experimental protocol, data processing algorithm, and processing of the experimental data. The Ministry of Science and Higher Education of the Russian Federation (Project No. 8.2501.2017/4.6 supported this research in terms of the videocapillaroscopy system developing and manufacturing, data preparation, and preliminary data processing.

Disclosures

The authors declare that there are no conflicts of interest related to this article.

References

1. B. Fagrell and M. Intaglietta, "Microcirculation: its significance in clinical and molecular medicine," J. Intern. Med. **241**(5), 349–362 (1997).

Biomedical Optics EXPRESS

2. S. Erikkson, J. Nilsson, and C. Sturesson, "Non-invasive imaging of microcirculation: a technology review," Med. Devices: Evidence Res. **7**, 445–452 (2014).
3. C. Lal and M. J. Leahy, "An updated review of methods and advancements in microvascular blood flow imaging," Microcirculation **23**(5), 345–363 (2016).
4. P. Butti, M. Intaglietta, H. Reimann, C. Holliger, A. Bollinger, and M. Anliker, "Capillary red blood cell velocity measurements in human nailfold by videodensitometric method," Microvasc. Res. **10**(2), 220–227 (1975).
5. M. V. Volkov, N. B. Margaryants, A. V. Potemkin, M. A. Volynsky, I. P. Gurov, O. V. Mamontov, and A. A. Kamshilin, "Video capillaroscopy clarifies mechanism of the photoplethysmographic waveform appearance," Sci. Rep. **7**(1), 13298 (2017).
6. F. Ingegnoli, R. Gualtierotti, C. Lubatti, C. Bertolazzi, M. Gutierrez, P. Boracchi, M. Fornili, and R. De Angelis, "Nailfold capillary patterns in healthy subjects: A real issue in capillaroscopy," Microvasc. Res. **90**, 90–95 (2013).
7. M. Cutolo, A. Sulli, and V. Smith, "How to perform and interpret capillaroscopy," Best Pract. Res. Clin. Rheumatol. **27**(2), 237–248 (2013).
8. E. H. B. M. Gronenschild, D. M. J. Muris, M. T. Schram, U. Karaca, C. D. A. Stehouwer, and A. J. H. M. Houben, "Semi-automatic assessment of skin capillary density: Proof of principle and validation," Microvasc. Res. **90**, 192–198 (2013).
9. M. Cutolo, A. C. Trombetta, K. Melsens, C. Pizzorni, A. Sulli, B. Ruaro, S. Paolino, E. Deschepper, and V. Smith, "Automated assessment of absolute nailfold capillary number on videocapillaroscopic images: Proof of principle and validation in systemic sclerosis," Microcirculation **25**(4), e12447 (2018).
10. E. C. LeRoy and T. A. Medsger Jr., "Criteria for the classification of early systemic sclerosis," J. Rheumatol. **28**(7), 1573–1576 (2001).
11. I. S. Sidorov, M. A. Volynsky, and A. A. Kamshilin, "Influence of polarization filtration on the information readout from pulsating blood vessels," Biomed. Opt. Express **7**(7), 2469–2474 (2016).
12. A. A. Kamshilin, E. Nippolainen, I. S. Sidorov, P. V. Vasilev, N. P. Erofeev, N. P. Podolian, and R. V. Romashko, "A new look at the essence of the imaging photoplethysmography," Sci. Rep. **5**(1), 10494 (2015).
13. I. P. Gurov, M. V. Volkov, N. B. Margaryants, A. Pimenov, and A. V. Potemkin, "High-speed video capillaroscopy method for imaging and evaluation of moving red blood cells," Opt. Lasers Eng. **104**, 244–251 (2018).
14. J. Allen, "Photoplethysmography and its application in clinical physiological measurement," Physiol. Meas. **28**(3), R1–R39 (2007).
15. A. A. Kamshilin, I. S. Sidorov, L. Babayan, M. A. Volynsky, R. Giniatullin, and O. V. Mamontov, "Accurate measurement of the pulse wave delay with imaging photoplethysmography," Biomed. Opt. Express **7**(12), 5138–5147 (2016).
16. A. V. Moço, S. Stuijk, and G. de Haan, "Motion robust PPG-imaging through color channel mapping," Biomed. Opt. Express **7**(5), 1737–1754 (2016).
17. S. Shin, Y. Yang, and J.-S. Suh, "Measurement of erythrocyte aggregation in a microchip stirring system by light transmission," Clin. Hemorheol. Microcirc. **41**(3), 197–207 (2009).
18. M. Hahn, T. Klysz, and M. Junger, "Synchronous measurements of blood pressure and red blood cell velocity in capillaries of human skin," J. Invest. Dermatol. **106**(6), 1256–1259 (1996).
19. M. Roustit and J.-L. Cracowski, "Assessment of endothelial and neurovascular function in human skin microcirculation," Trends Pharmacol. Sci. **34**(7), 373–384 (2013).
20. B. I. Levy, E. L. Schiffrin, J.-J. Mourad, D. Agostini, E. Vicaut, M. E. Safar, and H. A. Struijker-Boudier, "Impaired tissue perfusion: a pathology common to hypertension, obesity, and diabetes mellitus," Circulation **118**(9), 968–976 (2008).
21. M. Shibasaki, D. A. Low, S. L. Davis, and C. G. Crandall, "Nitric oxide inhibits cutaneous vasoconstriction to exogenous norepinephrine," J. Appl. Physiol. **105**(5), 1504–1508 (2008).